



Contents lists available at ScienceDirect

## Journal of Orthopaedic Translation

journal homepage: [www.journals.elsevier.com/journal-of-orthopaedic-translation](http://www.journals.elsevier.com/journal-of-orthopaedic-translation)

## Original article

## Bilayered scaffold with 3D printed stiff subchondral bony compartment to provide constant mechanical support for long-term cartilage regeneration



Tao Yang<sup>a,b</sup>, Maryam Tamaddon<sup>f</sup>, Le Jiang<sup>c,d</sup>, Jing Wang<sup>e,g</sup>, Ziyu Liu<sup>f</sup>, Zhongqun Liu<sup>c,d</sup>, Haoye Meng<sup>e</sup>, Yongqiang Hu<sup>e</sup>, Jianming Gao<sup>e</sup>, Xuan Yang<sup>e</sup>, Yanxu Zhao<sup>e</sup>, Yanling Wang<sup>c,d</sup>, Aiyuan Wang<sup>e</sup>, Qiong Wu<sup>h</sup>, Chaozong Liu<sup>f</sup>, Jiang Peng<sup>e</sup>, Xiaodan Sun<sup>c,d,\*\*</sup>, Qingyun Xue<sup>a,b,\*</sup>

<sup>a</sup> Peking University Fifth School of Clinical Medicine, Beijing, China<sup>b</sup> Department of Orthopaedics, Beijing Hospital, National Center of Gerontology, Institute of Geriatric Medicine, Chinese Academy of Medical Sciences, China<sup>c</sup> State Key Laboratory of New Ceramics and Fine Processing, School of Materials Science and Engineering, Tsinghua University, Beijing, China<sup>d</sup> Key Laboratory of Advanced Materials of Ministry of Education of China, School of Materials Science and Engineering, Tsinghua University, Beijing, China<sup>e</sup> Department of Orthopedic Surgery, Key Laboratory of Musculoskeletal Trauma & War Injuries PLA, Beijing Key Lab of Regenerative Medicine in Orthopedics, Chinese PLA General Hospital, Beijing, China<sup>f</sup> Institute of Orthopaedic & Musculoskeletal Science, University College London, Royal National Orthopaedic Hospital, Stanmore, HA7 4LP, UK<sup>g</sup> Yijishan Hospital, The First Affiliated Hospital of Wannan Medical College, No. 2, Zheshan West Road, Wuhu, Anhui, China<sup>h</sup> School of Life Sciences, Tsinghua University, Beijing, 100084, People's Republic of China

## ARTICLE INFO

## Keywords:

Bilayered scaffold  
Osteochondral repair  
Long-term cartilage repair  
Biomechanical microenvironment  
3D printing

## ABSTRACT

**Background/Objective:** We seek to figure out the effect of stable and powerful mechanical microenvironment provided by Ti alloy as a part of subchondral bone scaffold on long-term cartilage regeneration.

**Methods:** we developed a bilayered osteochondral scaffold based on the assumption that a stiff subchondral bony compartment would provide stable mechanical support for cartilage regeneration and enhance subchondral bone regeneration. The subchondral bony compartment was prepared from 3D printed Ti alloy, and the cartilage compartment was created from a freeze-dried collagen sponge, which was reinforced by poly-lactic-co-glycolic acid (PLGA).

**Results:** *In vitro* evaluations confirmed the biocompatibility of the scaffold materials, while *in vivo* evaluations demonstrated that the mechanical support provided by 3D printed Ti alloy layer plays an important role in the long-term regeneration of cartilage by accelerating osteochondral formation and its integration with the adjacent host tissue in osteochondral defect model at rabbit femoral trochlea after 24 weeks.

**Conclusion:** Mechanical support provided by 3D printing Ti alloy promotes cartilage regeneration by promoting subchondral bone regeneration and providing mechanical support platform for cartilage synergistically.

**Translational potential statement:** The raw materials used in our double-layer osteochondral scaffolds are all FDA approved materials for clinical use. 3D printed titanium alloy scaffolds can promote bone regeneration and provide mechanical support for cartilage regeneration, which is very suitable for clinical scenes of osteochondral defects. In fact, we are conducting clinical trials based on our scaffolds. We believe that in the near future, the scaffold we designed and developed can be formally applied in clinical practice.

## 1. Introduction

Cartilage injury commonly caused by joint disease, trauma or aging will seriously affect the quality of patients' life. Worsely, due to its low cellular and nonvascular properties, cartilage has limited self-healing

ability. Cartilage or joint reconstruction is still a considerable challenge due to cartilage injury, which leads to severe pain and disability of joint inflammation [1–5]. The increasing clinical demands has driven a large number of clinical surgical treatments, including autografts transplantation [6], autologous chondrocyte transplantation [7], and marrow

\* Corresponding author.

\*\* Corresponding author. State Key Laboratory of New Ceramics and Fine Processing, School of Materials Science and Engineering, Tsinghua University, Beijing, China.

E-mail addresses: [sunxiaodan@tsinghua.edu.cn](mailto:sunxiaodan@tsinghua.edu.cn) (X. Sun), [xueqingyun0433@bjhmoh.cn](mailto:xueqingyun0433@bjhmoh.cn) (Q. Xue).<https://doi.org/10.1016/j.jot.2021.09.001>

Received 22 April 2021; Received in revised form 29 August 2021; Accepted 2 September 2021

stimulation such as microfracture [8] and subchondral drilling [9]. Although successful to some extent, each treatment has its own limitations. For instance, marrow transplantation can lead to the formation of fibrocartilage [10], while autografts transplantation may have problems such as donor site morbidity and incomplete integration between grafts and host tissue [11].

Tissue engineering (TE) has provided a promising alternative option to current surgical treatments of cartilage injury, overcoming some of the limitations of the current approaches [12]. However, clinical studies have shown that articular cartilage injury always goes deep into subchondral bone, resulting in osteochondral defect of the knee joint, which changes the biomechanical properties of the joint and affects the long-term performance of the cartilage tissue [13], indicating that the full-thickness simultaneous repair of the cartilage layer and subchondral bone layer is of great significance for the successful repair of the knee joint [14]. Moreover, cartilage and subchondral bone have different composition, structural, biochemical and biomechanical properties. For example, it has been suggested that the pore size of scaffold conducive to cartilage regeneration is 30–100  $\mu\text{m}$ , while a larger pore size is needed to allow blood vessels to grow in for bone tissue [15]. The complex preparation techniques to realize the gradient structure and composition, limit their further application in osteochondral tissue engineering. 3D printing can provide desired pore size and fiber diameter, facilitate tissue growth and integration, and customize personalized scaffold for each patient.

Although the synthetic and natural polymers, bioceramic, bioglasses as well as decellularized ECM-derived scaffold biomaterials have shown promising results to provide functional osteochondral constructs in short-term [16,17], the decreased mechanical strength of these biodegradable scaffolds as subchondral bone scaffolds could impair the structure of the newly formed cartilage and provide insufficient mechanical support for cartilage regeneration in long-term [18–20]. It has been shown that severe bone mineral density loss, hence less support for cartilage, will lead to further cartilage damage, which will lead to arthritis in clinical [21]. Traditional titanium implants, with or without apatite coating, could be used for repair bone in traditional application [22,23].

In this study, we developed a bilayered osteochondral scaffold based on the assumption that a stiff subchondral bony compartment would enhance bone and cartilage regeneration in long-term. The bony compartment was 3D printed macroporous titanium alloy scaffolds, which are used to provide essential mechanical support for cartilage regeneration in long-term, while the cartilage compartment was created from a freeze-dried collagen sponge with micropores for better cartilage regeneration, which was infiltrated with poly-lactic-co-glycolic acid (PLGA) to improve its mechanical properties [24–27]. The results demonstrated that the 3D printed Ti alloy can not only accelerate bone formation and integration with the adjacent host tissue, but also induce better cartilage regeneration in osteochondral defect model at rabbit femoral trochlea after 24 weeks by providing the sufficient and steady mechanical support.

Herein, we provide a new scheme of bilayered scaffold that combines 3D printed stiff bony compartment and biodegradable cartilage compartment for long-term cartilage repair, which has enormous potential for further clinical application.

## 2. Materials and methods

### 2.1. Scaffold fabrication and characterization

The bilayered osteochondral scaffold was prepared using a Ti alloy as the bony compartment and a collagen-poly(lactic co glycolic acid) (PLGA) sponge as the cartilage compartment. Ti-based lattice corresponding to the bony compartment of the scaffold was manufactured from titanium alloy powder (EOS Ti<sub>6</sub>Al<sub>4</sub>V, Germany) using a Direct Metal Laser Sintering system (DMLS, EO SINTM270) as previously described [28]. The designed porosity of Ti<sub>6</sub>Al<sub>4</sub>V scaffolds was 59.08%. Type-I acid-soluble

collagen (Lando Biomaterials, China) was crosslinked using EDC/NHS as described before [29] and poured into the custom-made moulds either on top of the Ti-based lattice or by itself. The obtained Ti<sub>6</sub>Al<sub>4</sub>V-collagen assembly was freeze-dried (Christ Alpha 1-2LD, UK) before freezing at  $-20\text{ }^{\circ}\text{C}$  overnight. A 10 wt% PLGA solution was made by dissolving PLGA powder (Resomer RG 858 S, Evonik, Germany) in acetone (VWR, UK). The collagen layer was infiltrated with PLGA solution and the assembly was dried using a critical point dryer (Emitech K850, UK). The final samples were oven-dried at  $59\text{ }^{\circ}\text{C}$  overnight to ensure the complete removal of acetone. The diameter of the scaffold is 4 mm, and the height of the Ti<sub>6</sub>Al<sub>4</sub>V layer and c-PLGA layer is 4 mm and 2 mm respectively. The porous cylindrical titanium alloy scaffold with a height of 4 mm was fabricated by additive manufacturing. The scaffold is composed of 0.5 mm titanium alloy round rods, with a local distance of 0.5 mm and a layer spacing of 0.5 mm. The samples were then sterilized by gamma irradiation at 25 kGy (Synergy Health, UK) before evaluations *in vitro* or *in vivo*. The adhesion strength between Ti<sub>6</sub>Al<sub>4</sub>V and c-PLGA layers was examined by using a modified shear test (Emco F1 CNC). The Ti<sub>6</sub>Al<sub>4</sub>V part of the sample was held in a custom-made holder, while the force was applied to the c-PLGA layer using a custom-made curved endcap at a rate of 2 mm/min.

Field Emission Scanning Electron Microscope (FESEM, Merlin, Zeiss, Germany, SE2) was used to observe the micromorphology of scaffolds (EHT = 15 kV for Ti<sub>6</sub>Al<sub>4</sub>V layer, EHT = 5 kV for c-PLGA layer). Raman spectrum was measured by the micro-Raman system (i-Raman Plus) that is made by B&W TEK Inc., with the excitation wavelength of 785 nm. The stress-strain curve was tested in compression with a Zwick Roell Z0.5 (Germany) device at 0.8 mm/min in the dry state.

### 2.2. Cell compatibility and proliferation *in vitro*

#### 2.2.1. Bone marrow mesenchymal stem cell isolation and characterization

Bone marrow stem cells (BMSCs) were obtained from randomly selected 6–8 weeks-old Sprague–Dawley male rats. After euthanasia by sodium pentobarbital and cervical dislocation, bone marrow was flushed out of the femur and tibia with pre-cooled PBS sterile solution (Solarbio, china) several times. The bone marrow was centrifuged at 1500 g for 10 min, followed by filtration with 200 mesh aseptic stainless-steel screen to remove impurities under standard sterile conditions. After centrifugation at 1500g for 10 min, the cell suspension was obtained by removing the supernatant liquid. The cells were then plated in 25 cm<sup>2</sup> flasks (Corning, USA) and 5 ml of low glucose DMEM cell culture medium (Corning, USA) containing 10% FBS (Corning, USA) was added and incubated in a humidified atmosphere of 5% CO<sub>2</sub> at 37  $^{\circ}\text{C}$ . The culture medium was changed every 2 days until 80% confluent. The cells were then passaged and used for experiments at the second or third passage. The ability of BMSCs to differentiate into osteoblasts, chondrocytes, and adipocytes was examined by tri-lineage differentiation and staining with Alizarin Red, Alcian Blue, and Oil Red O, respectively.

#### 2.2.2. Cell Proliferation of BMSCs in scaffolds' extract

The proliferation of BMSCs within each extract was measured using the CCK-8 assay (Dojindo Molecular Technologies, Kumamoto, Japan). The BMSCs were cultured in 96-well plates (Corning, USA) at  $5.0 \times 10^6$  cells/L with the cell culture medium. After 2 h to allow for the cell adhesion, the sample extracts were added to each well for 1, 3, 5, and 7 days. On the following days, cell proliferation was measured using the CCK8 assay as described by the manufacturer. For CCK-8 measurement, the absorbance of the culture medium was measured at 450 nm using a microplate reader (Dojindo, Japan).

#### 2.2.3. Cell compatibility of Ti<sub>6</sub>Al<sub>4</sub>V scaffold

Cytocompatibility of Ti<sub>6</sub>Al<sub>4</sub>V scaffolds was assessed by FDA (Fluorescein diacetate) and PI (Propidium iodide) staining. The titanium alloy cylinder scaffold was placed in the well plate with the axial direction perpendicular to the bottom of the well plate, then the cells were

cultured. CLSM was used to image the cells on the round surface of the top of the titanium alloy cylinder. The samples were incubated in 1 ml of PBS containing 1  $\mu$ L of FDA and 1  $\mu$ L of PI stock solution (diluted 1000 times) for 15 min, followed by rinsing with PBS. The samples were then imaged under a fluorescence microscope (Olympus, Japan).

### 2.3. Surgical procedure and scaffold implantation

In vivo assessment was carried out in a rabbit model and conducted under the approval of and in compliance with the Ethics Committee of the Chinese PLA General Hospital, Beijing, China. A total of thirty 3-months New Zealand white male rabbits with the weight of 2.0–2.5 kg were used in this study. The anesthetic was induced with 3% sodium pentobarbital. Distal femoral trochlea of the knee joint was exposed through a medial longitudinal skin incision and parapatellar approaches to the joint and followed by blunt dissection of the capsule. Cylindrical critical size osteochondral defects (diameter: 4 mm, height: 6 mm) were created in the distal femoral trochlea and the appropriate scaffolds were implanted into the created defect. The samples were divided into three groups:

- 1) Control group (n = 9, control): empty defect without any scaffold;
- 2) cPLGA group (n = 9, control): monolayer collagen-PLGA scaffold;
- 3) Bilayer group (n = 12, experimental): Bilayered Ti<sub>6</sub>Al<sub>4</sub>V + collagen-PLGA scaffold.

At 4, 12 and 24 weeks post-surgery, the rabbits were euthanized by injection of 90–120 mg/kg of bodyweight sodium pentobarbital via the ear vein. Femoral trochleae were harvested for further analysis. After macroscopic evaluations, the samples were fixed in 10% formalin for the remainder of analyses. MicroCT and mechanical testing on cartilage were performed and then the samples were cut in half from the middle of the implant using a diamond saw system (EXAKT-300CP). Half of each sample was processed for histology and the other half was used for mechanical evaluation of regenerated bone.

### 2.4. Macroscopic evaluations

The excised samples were stripped of soft tissues for macroscopic evaluation. Each sample was evaluated for any signs of inflammation or adhesions. The macroscopic appearance and quality of cartilage healing were blindly assessed using the criteria set by the International Association for cartilage Research (International Cartilage Research Society, ICRS) [30].

### 2.5. Histological evaluations

The harvested tissues were fixed in 10% formalin (Solarbio, China) for 48 h, and dehydrated through a series of alcohol (70%–95%) for 24 h. The samples were placed in anhydrous alcohol and resin solutions (Technovit 7200) with the ratio of 3:7 and 1:1 for 2 days respectively and then were moved to pure resin solution (3 and 7 days). Afterward, samples were embedded in resin using UV light and sectioned into 200  $\mu$ m thickness with a hard tissue microtome (German EXAKT300CP). Finally, the sections were reduced and polished to 20  $\mu$ m by using a polisher (German EXAKT 400 S) and were stained with Hematoxylin and Eosin (H&E) and Toluidine blue.

### 2.6. Mechanical evaluation of regenerated tissue

#### 2.6.1. Nano-compression of repaired cartilage

The Young's Modulus of the regenerated cartilage was measured by Nano-indenter (Piuma Nano-indenter, Netherlands) and calculated using a Hertzian model of the data on the loading section of the load-

indentation data curve [31]. Measurement Parameters were as follow: Probe Stiffness: 0.48 N/m; Probe Radius: 53  $\mu$ m; Speed: 5  $\mu$ m/s; Indenter Type: sphere.

#### 2.6.2. Nano-compression of regenerated bone

The mechanical properties of two areas (center and periphery) of the new bone were tested by nano-compression test machine (G200 nano indenter, KLA-USA). The central area of the new bone was tested by dynamic compression model [32] using a cylindrical indenter with 3 mm of maximum dynamic indentation depth, and 1 HZ oscillation frequency. Due to the high content of water and soft nature of the regenerated bone in the centre, the dynamic method was able to prevent the influence of the material's viscoelasticity on the elasticity measurement. The periphery area of the new bone was more solid and a static model with a triangular pyramid indenter and 3 mm maximum indentation depth was used. The load-indentation depth curves were recorded [33] for calculating elastic modulus.

### 2.7. Micro-CT analysis

Micro-CT analysis was performed on all samples using a GE eXplore Locus with 80 kV X-ray source and 175  $\mu$ A. The CT slice was 45  $\mu$ m thick and pixel size was 45\*45  $\mu$ m<sup>2</sup> to assess the quantity and structure of the new bone formed within the defect site. Three-dimensional (3D) reconstructions were performed using GE eXplore micro-CT and subsequently visualization was performed in Micro-View software (Built-in software). Mimics software (Materialise, Belgium) was used for the 3D reconstruction of the scaffold.

### 2.8. Statistical analysis

Statistical analysis was performed using the IBM SPSS 22.0 software (IBM, Armonk, NY, USA). All quantitative data were expressed as mean  $\pm$  standard deviation (n = 3, mean  $\pm$  SD) unless specified otherwise. For each normally distributed parameter, statistical analysis was performed using one-way analysis of variance (ANOVA) with t-test and a value of p < 0.05 \* or p < 0.01 \*\* was considered as statistically significant.

## 3. Results

### 3.1. Characterization of bilayered scaffold

As it can be seen, the pore and strut sizes of Ti<sub>6</sub>Al<sub>4</sub>V layer were both 0.5 mm as designed (Fig. 1A, C), SEM combined with EDS element distribution can prove the element composition of the Ti<sub>6</sub>Al<sub>4</sub>V layer. SEM images demonstrate that the collagen-PLGA has a three-dimensional porous structure (Fig. 1B). The PLGA is represented by the ester group peak at 1770 cm<sup>-1</sup> and the asymmetrical stretching of the C–O–C band at 1046 cm<sup>-1</sup> [34], and the collagen is represented by the peak of 2940 cm<sup>-1</sup> and 1425 cm<sup>-1</sup> [35] (Fig. 1D).

The Stress–strain curves were used to calculate the compressive modulus of Ti alloy layer by linear regression of the initial linear regime of the curve. The compressive modulus (n = 3,  $\pm$ SD) of Ti and collagen-PLGA was 73  $\pm$  4.4 MPa and 1.46  $\pm$  0.9 MPa respectively (Fig. 1E). The adhesion strength was calculated to be 1.34  $\pm$  0.25 MPa.

### 3.2. In vitro cellular evaluation of scaffold

As it can be seen from Fig. 2A, the BMSCs have the ability to differentiate into osteoblasts, chondrocytes, and adipocytes. CCK-8 kit was used for the evaluation of cell proliferation at 1, 3, 5, and 7 days. Cell proliferation studies further showed that the cells grew fast on both the Ti<sub>6</sub>Al<sub>4</sub>V layer and cPLGA layer (Fig. 1F). The cell compatibility of each

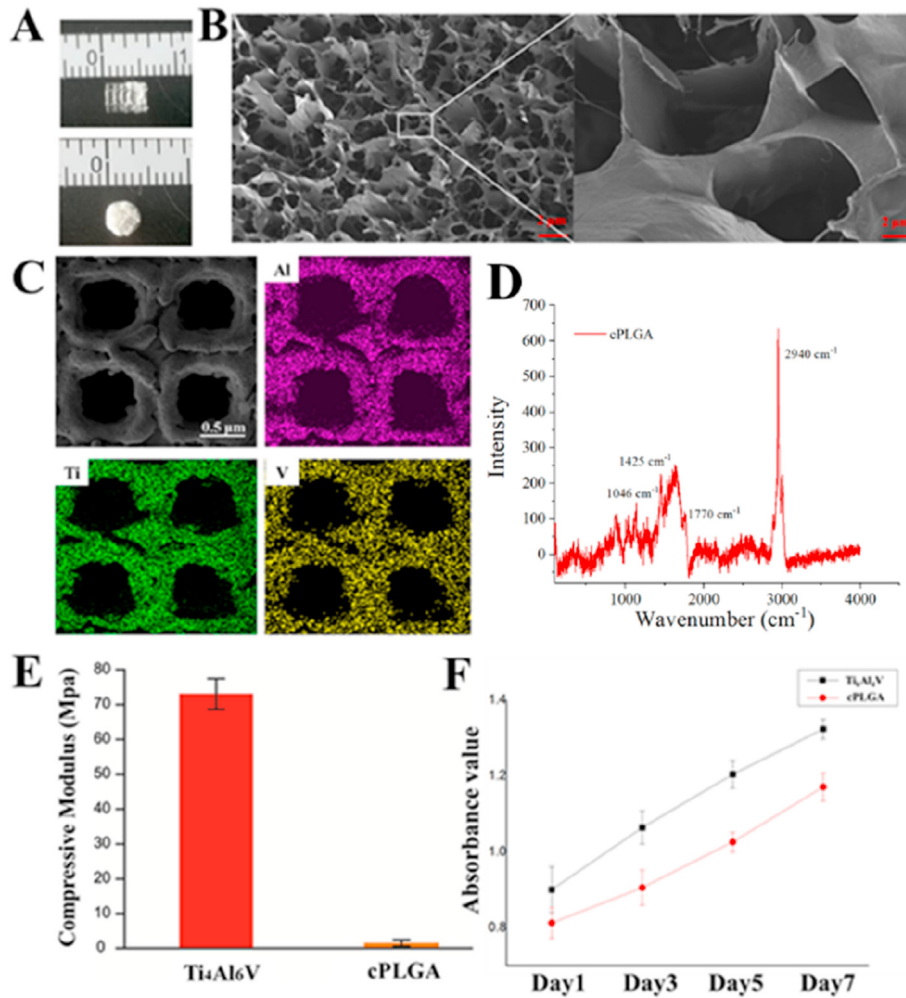


**Fig. 1.** Characterization of bilayered scaffold. A) macroscopical photos of bilayered scaffold, B) SEM image of cPLGA layer, C) SEM image and element distribution of Ti<sub>6</sub>Al<sub>4</sub>V layer, D) Raman spectrum of cPLGA, E) Compressive modulus of both layer, F) Absorbance of formazan (OD 450 nm) with scaffold at 1, 3, 5, 7 days,

layer of the scaffold was assessed for up to 7 days using Live/Dead assay. As shown in Fig. 2B, a large number of live cells (green) were located on each layer, with their number increasing over time (from day 1–7), demonstrating cell compatibility of the scaffold.

### 3.3. Superior repair in bilayer group by macroscopic observation

A rabbit model was used to evaluate the osteochondral repair capability for bilayered scaffolds. The general macroscopic views of tissue repair in all three groups at 1, 3, and 6 months are shown in Fig. 3A. In the control group and cPLGA group, the defect areas were incompletely filled by the repaired tissue, and the boundary between the defect and the normal tissue was obvious. Although as time progressed, the tissue filling in the defect area gradually improved, the boundary remained visible, and the surface of the new tissue was not glossy as should be in normal hyaline cartilage. In contrast, the defect area of the bilayer group was gradually filled with a new tissue whose boundary was highly intertwined with the normal tissue showing better tissue integration [36,37]. Although the cartilage defect at 6 months was still not completely repaired with small strip-shaped defect, the repair of bilayer group was significantly better compared with the cPLGA group and the control group as shown in Fig. 3B. Interestingly, the histological score of subchondral bone tissue decreased significantly at 24 weeks compared with

12 weeks (Fig. 3C). At 24 weeks, the histological score of subchondral bone in the bilayer group was significantly higher than that in the other two groups (Fig. 3C), and it also showed good repair effect even in the center of the scaffold (Fig. 4A). Moreover, no obvious inflammation was found in the animal tissues, which can be seen in Fig. 2A [38]. In addition, H&E sections in Fig. 5 also showed no obvious inflammation.

### 3.4. Mechanical properties of regenerated subchondral bone and cartilage

The compressive elastic modulus of the new tissue at center and border of scaffold and normal bone trabecular tissue were measured at 4, 12 and 24 weeks after implanting bilayered scaffold (Fig. 4B). We observed that the elastic modulus of the new tissue in the central area of the scaffold was significantly lower than that of the normal bone at all time points. However, the elastic moduli of the new tissue at the border of the scaffold were significantly higher than those of the central area and were closer to the natural bone. Although the elastic modulus of the new bone had not yet reached the level of natural bone, there were no significant statistical differences at 12 and 24 weeks.

The mechanical elastic moduli of cartilage tissue in the defect area were measured in the cPLGA and bilayered scaffold group and the surrounding native cartilage tissue at 24 weeks after implantation using nano-indentation. It can be observed in Fig. 4C that although Young's

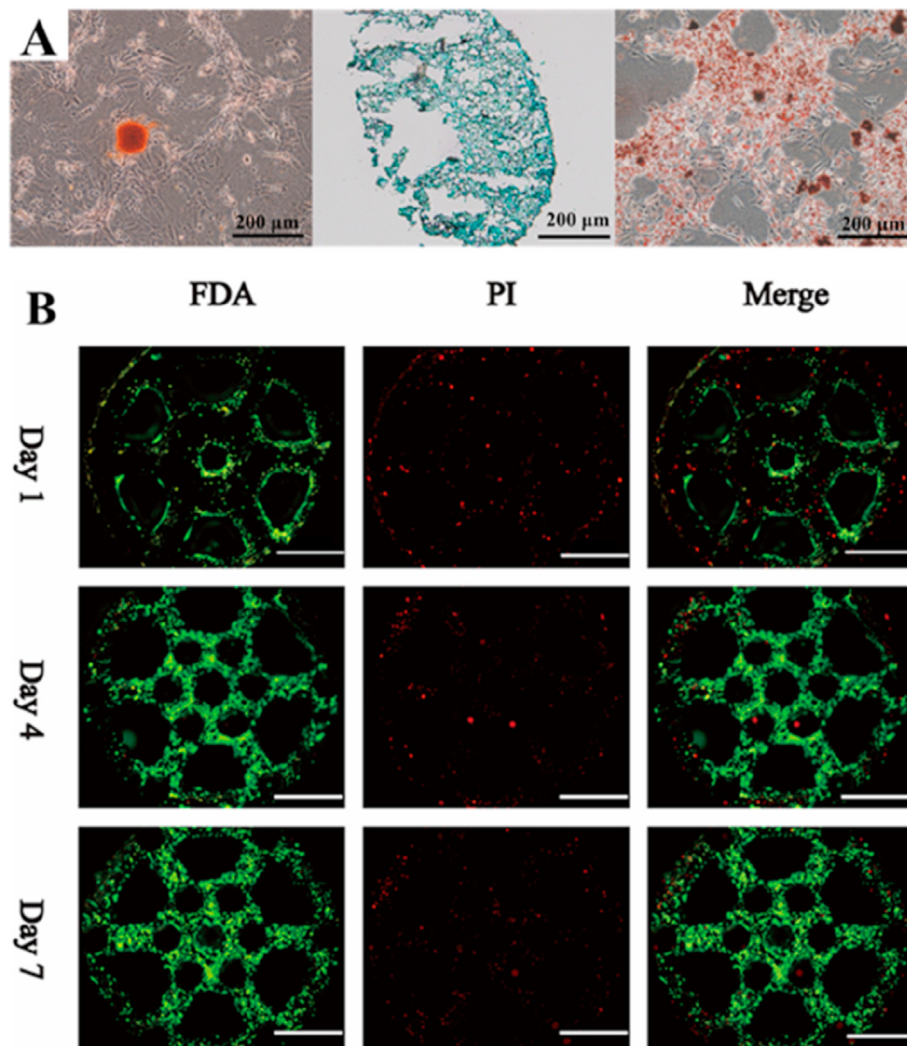


Fig. 2. A) Osteogenic differentiation, Chondrogenic differentiation, Adipogenic differentiation (from left to right), B) Immunofluorescence Live (FDA)/Dead (PI) staining of BMSCs cultured on Ti<sub>6</sub>Al<sub>4</sub>V scaffold at 1, 4, 7 days (the scale bar is 1 mm).

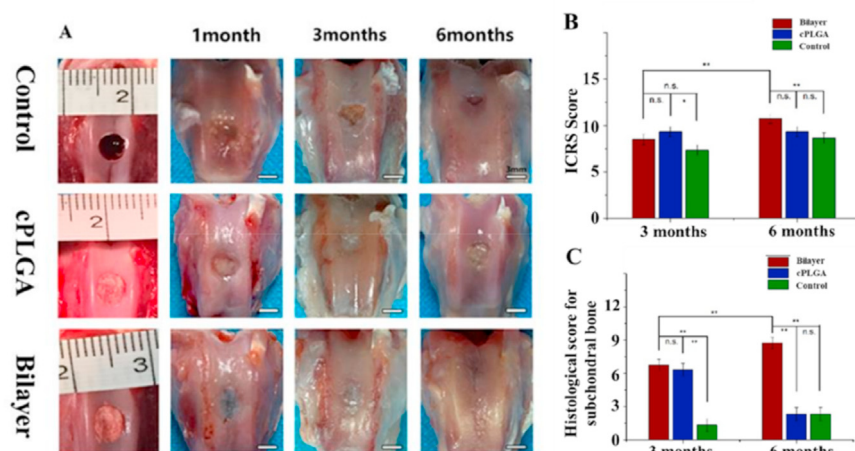
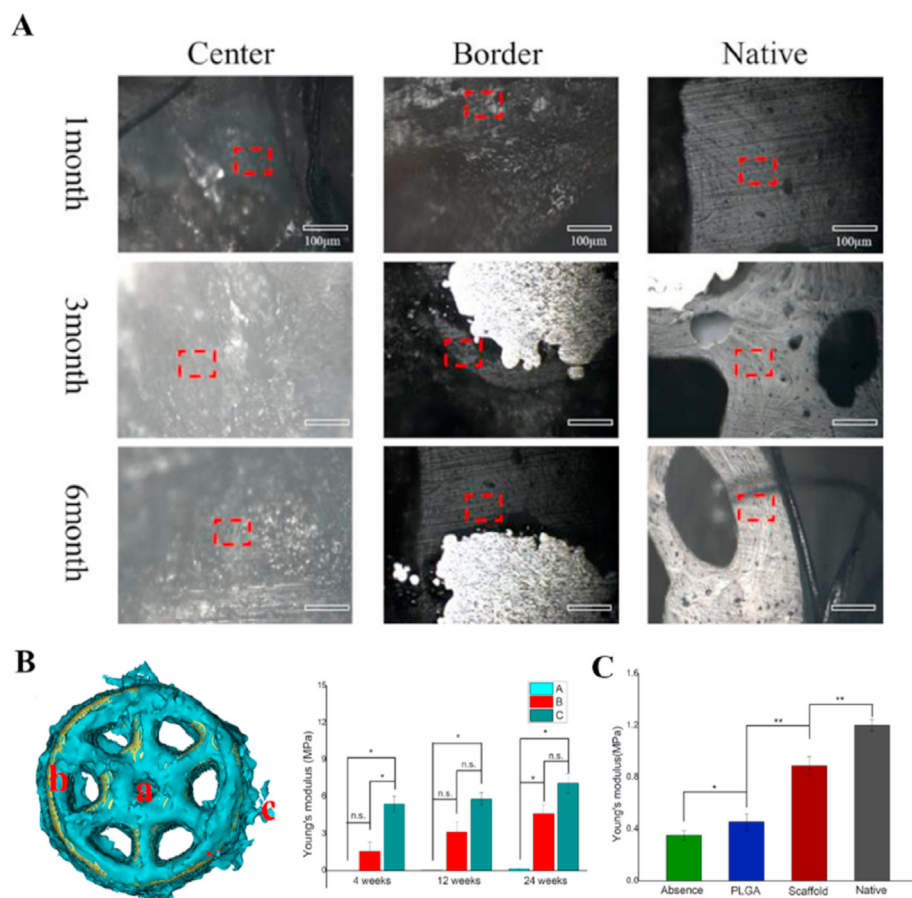


Fig. 3. Macroscopic evaluation and biomechanical properties of repaired knees. A) The gross observation of rabbit articular osteochondral defect repair with control, cPLGA and bilayer groups at 4, 12, 24 weeks after implantation (the scale bar is 3 mm). B) The diagram of general view scores quantitative analysis of articular cartilage after repair. C) Histological score for subchondral bone evaluation after repair. \*  $p < 0.05$ ; \*\*  $p < 0.01$ ; and n.s. represents no significant difference.



**Fig. 4.** Biomechanical evaluation of new subchondral bone and cartilage. A) The images of the scaffold group at 4, 12 and 24 weeks after implantation, were observed under 250x with built-in microscope of the nano-indenter. B) quantitative analysis of Young's modulus of representative the regenerative bone tissue at the center of the scaffold(a), the border of the scaffold(b), the normal trabecular tissue around the scaffold(c). C) quantitative analysis of cartilage mechanical properties with Young's modulus (MPa). \*  $p < 0.05$ ; \*\*  $p < 0.01$ ; and n.s. represents no significant difference.

modulus of the regenerated cartilage in the bilayered scaffold group had not yet reached those of the native cartilage level, it is significantly higher than that of the monolayer cPLGA scaffold group.

### 3.5. Micro-CT analysis of new bone formation

The micro-CT data was used to analyze new bone formation in the defect regions as shown in Fig. 5A and B. The 3D reconstructed images demonstrated that there were new bone formations within the bone defect regions at 4, 12 and 24 weeks after surgery in the bilayer group, where a large amount of new bone tissue was present both on the surface and within the pores of the scaffold. However, the other two groups exhibited a deficiency of osteogenic properties and had less or no new bone tissue formation within subchondral defect regions.

At all time points, a significantly higher bone mineral density (BMD,  $689.36 \pm 25.65 \text{ mg/cm}^3$ ,  $789.50 \pm 59.78 \text{ mg/cm}^3$  and  $780.71 \pm 44.24 \text{ mg/cm}^3$ , at 4, 12, and 24 weeks respectively) and new bone volume fraction (bone volume/total volume, BV/TV ( $72.26 \pm 4.60\%$ ) ( $82.97 \pm 2.62\%$ ) and ( $85.75 \pm 6.08\%$ ) at 4, 12, and 24 weeks respectively) were found in the bilayer group compared to the other two groups (Fig. 5C and D). Moreover, although cPLGA group had higher BMD and BV/TV values than the control group, there was no significant statistical difference between cPLGA and the absence control group at 4 and 24 weeks. Interestingly, there is a decrease in BMD and BV/TV values from 12 weeks to 24 weeks in cPLGA group, whereas they increased over time in the other two groups. The values of trabecular thickness (Tb.Th) exhibited the same aforementioned phenomenon as those of BMD and BV/TV in all three groups (Fig. 5E). A lower trabecular separation (Tb.Sp  $0.16 \pm 0.02 \text{ mm}$ ;  $0.13 \pm 0.03 \text{ mm}$ ;  $0.16 \pm 0.03 \text{ mm}$ ) were found in bilayer group compared with cPLGA ( $0.89 \pm 0.09 \text{ mm}$ ;  $0.44 \pm 0.02 \text{ mm}$ ;  $0.75 \pm 0.28 \text{ mm}$ ) and control group ( $1.29 \pm 0.29 \text{ mm}$ ;

$0.97 \pm 0.15 \text{ mm}$ ;  $0.79 \pm 0.32 \text{ mm}$ ) (Fig. 5F) at 4, 12 and 24 weeks, respectively. Moreover, a higher trabecular number (Tb.N, 1/mm) were found in bilayer group compared with cPLGA and control group overall (Fig. 5G).

### 3.6. Histological evaluation of regenerated subchondral bone and cartilage

In terms of subchondral bone repair, histological evaluations (Fig. 6) showed that the bone defects in the control group were filled with fibrous tissue, with only a few cells at 12 and 24 weeks. Although cPLGA group demonstrated more bone cells, and a few areas of bone regeneration compared with control group, most of the defect areas were filled with fibrous tissue. Meanwhile, the bilayer group demonstrated good integration between scaffold and native tissues and better new bone tissues compared with the other two groups at both 12 and 24 weeks (see Fig. 7).

The cartilage defect in the control group was filled with fibrous tissue with very few cells at 12 weeks and a few more cells at 24 weeks and the integration of the newly formed tissue and the surrounding cartilage was poor. Compared with the absence control group, cPLGA group demonstrated more cells at both 12 and 24 weeks and better integration of newly formed tissue and native surrounding. Although the morphology of new chondrocytes was similar to native cartilage cells, it was difficult to see the typical cell lacuna structure of normal cartilage. Satisfyingly, there was a good integration between the regenerated tissue and the surrounding cartilage in the scaffold group at 24 weeks. Although the number of chondrocytes observed in the repair tissue was a little less than the surrounding native chondral tissue, the morphology of new chondrocytes was almost the same as the normal tissue and they were arranged in a typical chondrocyte lacuna structure. In addition, according to the previous studies, c-PLGA could be degraded in 2–3 month which is conducive to the cartilage regeneration [39]. It can be seen from Fig. 5

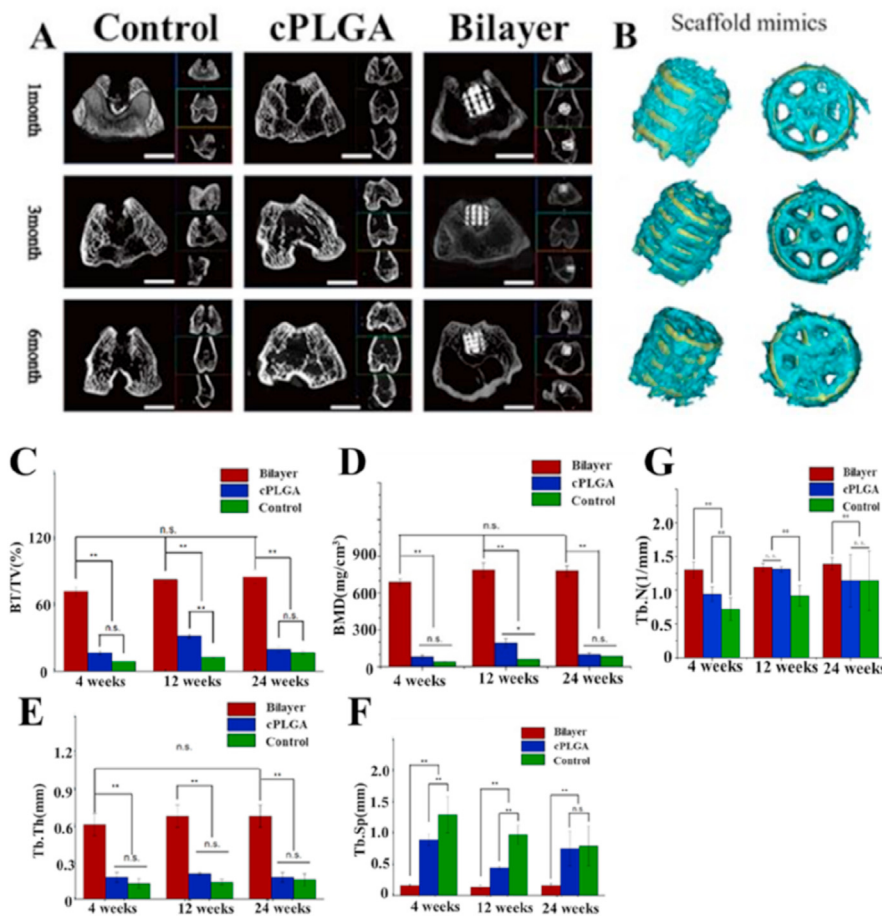


**Fig. 5.** Microcomputed tomography (micro-CT) evaluation. A: Representative two-dimensional micro-CT images at each time point (the scale bar is 5 mm). B: The graphic simulated 3D model of bilayer group based on dates of micro-CT scan performed by mimics software, which indicated majority of new bone tissues located on both the surface and pores of scaffold from both diagonally and vertically angle. The yellow represents scaffold materials. The green represents bone tissue. C-G): Quantitative analysis of micro-CT of the new bone formation in the implantation region at 4, 12, 24 weeks after surgery (C) BV/TV (D) BMD (E) Tb.Th (F) Tb.Sp (G) Tb.N; n = 3 in each group; \* p < 0.05; \*\* p < 0.01; and n.s. represents no significant difference.

that c-PLGA were almost completely degraded in 12 weeks, which is consistent with the reported studies.

#### 4. Discussion

Cartilage repair is an urgent clinical problem in orthopaedics. It has been demonstrated that targeting and repairing the whole osteochondral tissue but not just the cartilage may improve the outcome when using TE approaches. Bilayered TE scaffolds have been increasingly applied in the field of articular cartilage and osteochondral repair and have achieved good experimental results [40]. Considering the differences in the biochemical and biomechanical properties of cartilage and subchondral bone, the preparation of a functional bilayered scaffold could be relatively complex, and long-term repair of osteochondral defects remains a clinical challenge so far.

In this study, we developed a bilayered osteochondral scaffold based on the assumption that a stiff subchondral bone compartment would enhance bone and cartilage regeneration. We evaluated the scaffold *in vitro* to assess its biocompatibility and then compared this bilayered scaffold with a monolayered scaffold, identical to the upper layer of the bilayered scaffold, for the repair of osteochondral defects to verify the effects on the stiff subchondral bone compartment which can provide mechanical support on the regeneration of the cartilage.

The systematic assessment confirmed the regeneration of satisfactory hyaline-like cartilage and subchondral trabecular bone in the scaffold group by 24 weeks post-operation in rabbit, which indicates the potential of the scaffold for osteochondral defect repair. The *in vitro* experiments showed that both cPLGA layer and the porous Ti<sub>6</sub>Al<sub>4</sub>V layer exhibited good biocompatibility and no obvious biological toxicity. The mechanical testing of the Ti<sub>6</sub>Al<sub>4</sub>V layer as bony compartment of the bilayered

scaffold showed its compressive modulus is in the range of natural bone, which has been suggested that better mechanical match between implanted scaffold and native tissue may induce better regeneration and integration [38].

In the *in vivo* experiments, we observed the formation of a large amount of new bone tissue throughout the subchondral bone part of the scaffold, which integrated well with the adjacent native tissue. Similarly, BMD and Tb.th exhibited much higher values in the bilayer group compared to cPLGA group and control group and increased with implantation time. Despite the higher values of BV/TV and BMD in cPLGA group compared to the empty control group at 3 months, they interestingly decline with time, possibly showing that the absence of mechanical support from bony compartment in the cPLGA group may have had a detrimental effect on the maintenance of the tissue in long-term, which demonstrated the indispensable effect of mechanical support provided by the bony compartment.

At the same time, gross observation and ICRS scoring revealed that the bilayer group had better cartilage regeneration than cPLGA group and control group. Also, histological examinations demonstrated that the morphology of the cells in the cartilage of the bilayer group was more similar to the adjacent native chondrocytes, while both cPLGA group and bilayer group had neo tidemark-like formations, compared with the control group which had defective subchondral bone structure and mixed clusters cells. Moreover, the Young’s modulus of the neocartilage in the bilayer group was higher than that in the cPLGA group, which demonstrated the mechanical support from bone compartment played an important role in the regeneration of cartilage. These findings prove that an inferior repair of subchondral bone with insufficient biomechanical properties negatively impacts on the long-term performance of the chondral tissue repair [41].

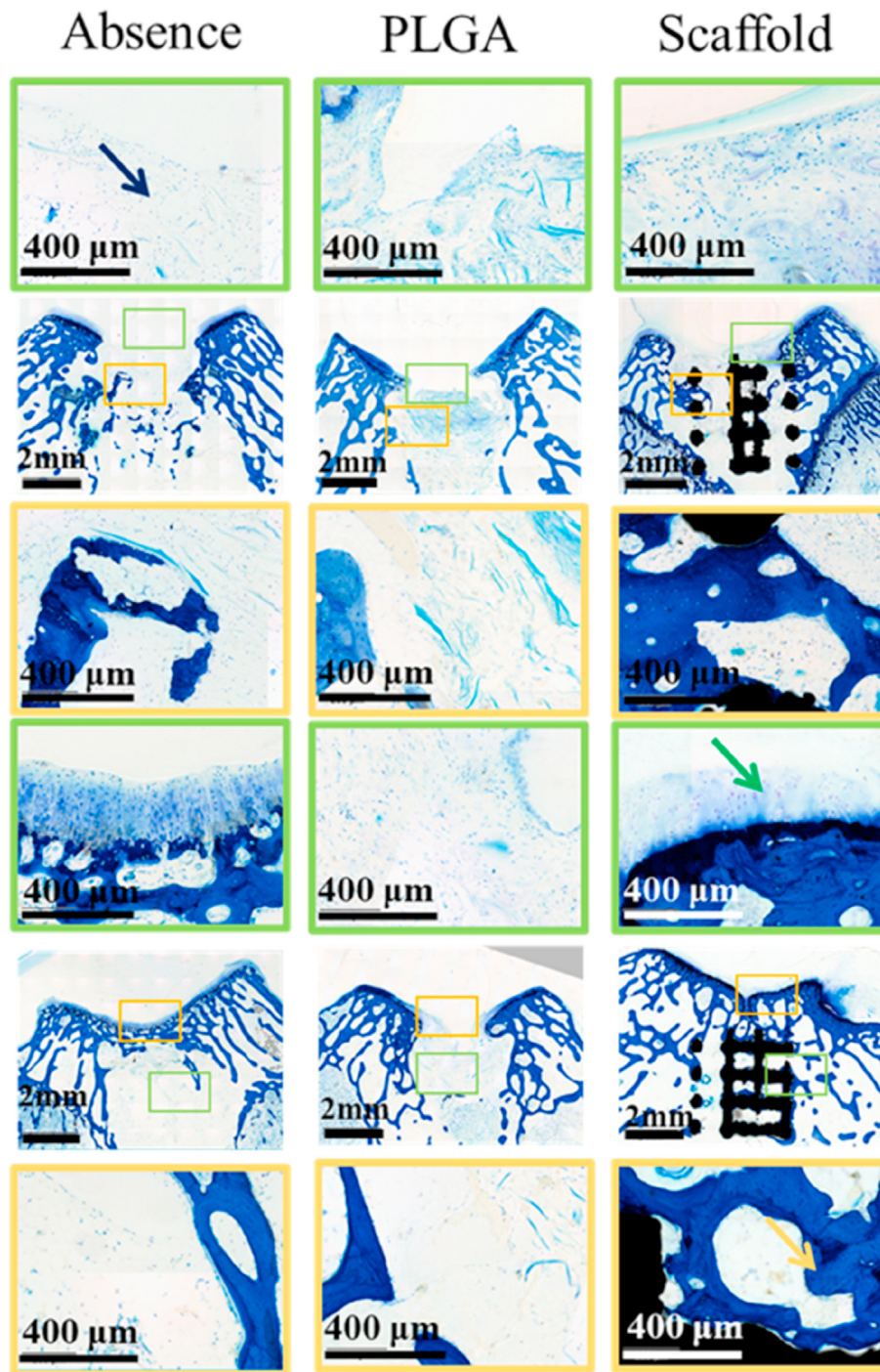


Fig. 6. Toluidine blue staining of the osteochondral samples and magnifications of new cartilage (yellow square frame denotes subchondral layer, green square frame denotes cartilage layer).

Postoperative trauma of the surgical procedure to implant a scaffold leads to a rapid influx of host MSCs and growth factors into the defect area [42]. It has been suggested that the growth of new cartilage tissue starts in the subchondral area, and as the ossification process progresses the new cartilage is moved up to the surface of the joint [15]. Stable mechanical support can prevent the growth of fibrous tissue and promote the formation of new bone tissue, which will be conducive to the regeneration of cartilage [6]. Meanwhile, stable mechanical support can

provide a stable mechanical platform, which is conducive to cartilage tissue regeneration [43]. Unfailing biomechanical support from the lower part of the defect might lead to a better ossification process and subsequently contribute to moving the cartilage up to the surface of the joint. Although how the specific type and regime of mechanical loading, as well as the mechano-transduction signaling, which affect chondrogenesis and ECM synthesis has yet to be clarified [44], we may be able to speculate that mechanics might be the trigger for osteochondral repair





**Fig. 7.** H&E staining of the osteochondral samples and magnifications of new cartilage (yellow square frame denotes subchondral layer, green square frame denotes cartilage layer).

through this study. Our research has proven that materials with unfailing mechanical strength can effectively promote the growth of trabecular bone tissue, which contributed to the development of cartilage. Therefore, it is rational to conclude that mechanical support may promote cartilage regeneration by promoting subchondral bone regeneration and providing a mechanical support platform for cartilage synergistically.

### 5. Conclusion

In summary, we successfully fabricated a porous bilayered scaffold for the long-term repair of osteochondral defects with a stiff subchondral bone compartment made of 3D printed Ti alloy, which was proven to play

an indispensable role in the regeneration of both bone and overlying cartilage. *In vitro* evaluations confirmed the biocompatibility of the scaffold materials. Furthermore, *in vivo* evaluations in the rabbit femoral joint at different time points showed significantly better bone and cartilage regeneration in the bilayered scaffold group when compared with a monolayered scaffold group without the Ti alloy layer. The macroscopic appearance of cartilage, as well as ICRS scoring, increased significantly with the amount of bone formation and bone mineral density. It was suggested that this bilayered scaffold has a potential to treat osteochondral defects by providing stable subchondral support for cartilage regeneration, and can be used in a one-step surgical procedure to address the current unmet clinical needs.

## Ethical approval

This study obtained written approval from the Ethics Committee of the Chinese PLA General Hospital, Beijing, China.

## Declaration of competing interest

The authors declare that they have no conflict of interest.

## Acknowledgement

This work was supported by the intergovernmental cooperation in science and technology (2016YFE0125300); National Key Research and Development Program of China (2016YFB0700802); Natural Sciences Foundation of China (52072210, 31670991); Major projects of the National Social Science Funding (17ZDA019); Tsinghua University Initiative Scientific Research Program (2019Z); and the Innovate UK and the Ministry of Science & Technology of China (A02872) and EC via H2020-MSCA-RISE programme (BAMOS, grant no: 734156).

## References

- Freedman BR, Mooney DJ. Biomaterials to mimic and heal connective tissues. *Adv Mater* 2019;31(19):1806695.
- Zhang B, Sun H, Wu L, Ma L, Xing F, Kong Q, et al. 3D printing of calcium phosphate bioceramic with tailored biodegradation rate for skull bone tissue reconstruction. *Bio-Design Manuf* 2019;2(3):161–71.
- Li X, Yuan Y, Liu L, Leung Y-S, Chen Y, Guo Y, et al. 3D printing of hydroxyapatite/tricalcium phosphate scaffold with hierarchical porous structure for bone regeneration. *Bio-Design Manuf* 2020;3(1):15–29.
- Duan W, Zhao Y, Ren X, Zhao R, Li Q, Sun Z, et al. Combination of chondrocytes and chondrons improves extracellular matrix production to promote the repairs of defective knee cartilage in rabbits. *J Orthop Transl* 2021;28:47–54.
- Xu G, Hu X, Han L, Zhao Y, Li Z. The construction of a novel xenograft bovine bone scaffold, (DSS)6-liposome/CKIP-1 siRNA/calcine bone and its osteogenesis evaluation on skull defect in rats. *J Orthop Transl* 2021;28:74–82.
- Marcacci M, Kon E, Delcogliano M, Filardo G, Busacca M, Zaffagnini S. Arthroscopic autologous osteochondral grafting for cartilage defects of the knee: prospective study results at a minimum 7-year follow-up. *Am J Sports Med* 2007;35:2014–21.
- Salzmann GM, Sauerbach M, Berninger MT, Kaltenhauser T, Schonfelder M, Vogt S, et al. The dependence of autologous chondrocyte transplantation on varying cellular passage, yield and culture duration. *Biomaterials* 2011;32:5810–8.
- Gobbi A, Karnatzikos G, Kumar A. Long-term results after microfracture treatment for full-thickness knee chondral lesions in athletes. *Knee Surg Sports Traumatol Arthrosc* 2014;22:1986–96.
- Eldracher M, Orth P, Cucchiariini M, Pape D, Madry H. Small subchondral drill holes improve marrow stimulation of articular cartilage defects. *Am J Sports Med* 2014;42:2741–50.
- Yang HS, La WG, Bhang SH, Kim H-J, Im G-I, Lee H, et al. Hyaline cartilage regeneration by combined therapy of microfracture and long-term bone morphogenetic protein-2 delivery. *Tissue Eng* 2011;17:1809–18.
- Hangody L, Dobos J, Baló E, Pánics G, Hangody LR, Berkes I. Clinical experiences with autologous osteochondral mosaicplasty in an athletic population: a 17-year prospective multicenter study. *Am J Sports Med* 2010;38:1125–33.
- Langer R, Vacanti JP. Tissue engineering. *Science* 1993;260:920–6.
- Armiento AR, Alini M, Stoddart MJ. Articular fibrocartilage - Why does hyaline cartilage fail to repair. *Adv Drug Deliv Rev* 2018;146:289–305.
- Liao S, Xu L, Hu L, Chen D, Yu L, Li X, et al. Stearic acid methyl ester promotes migration of mesenchymal stem cells and accelerates cartilage defect repair. *J Orthop Transl* 2020;22:81–91.
- Du Y, Liu H, Yang Q, Wang S, Wang J, Ma J, et al. Selective laser sintering scaffold with hierarchical architecture and gradient composition for osteochondral repair in rabbits. *Biomaterials* 2017;137:37–48.
- Nicodemus GD, Bryant SJ. The role of hydrogel structure and dynamic loading on chondrocyte gene expression and matrix formation. *J Biomech* 2008;41(7):1528–36.
- Jeon JE, Vaquette C, Klein TJ, Huttmacher DW. Perspectives in multiphasic osteochondral tissue engineering. *Anat Rec* 2014;297(1):26–35.
- Chung C, Beecham M, Mauck RL, Burdick JA. The influence of degradation characteristics of hyaluronic acid hydrogels on in vitro neocartilage formation by mesenchymal stem cells. *Biomaterials* 2009;30(26):4287–96.
- Duan P, Pan Z, Cao L, Gao J, Yao H, Liu X, et al. Restoration of osteochondral defects by implanting bilayered poly(lactide-co-glycolide) porous scaffolds in rabbit joints for 12 and 24 weeks. *J Orthop Transl* 2019;19:68–80.
- Ruvinov E, Tavor Re'em T, Witte F, Cohen S. Articular cartilage regeneration using acellular bioactive affinity-binding alginate hydrogel: a 6-month study in a mini-pig model of osteochondral defects. *J Orthop Transl* 2019;16:40–52.
- Mangnus L, van Steenberg HW, Reijnierse M, Kälvesten J, van der Helm-Van Mil AHM. Bone mineral density loss in clinically suspect arthralgia is associated with subclinical inflammation and progression to clinical arthritis. *Scand J Rheumatol* 2017;1–5.
- Mao C, Li H, Cui F, Feng Q, Ma C. The functionalization of titanium with EDTA to induce biomimetic mineralization of hydroxyapatite. *J Mater Chem* 1999;9(10):2573–82.
- Kim HJ, Han MA, Shin JY, Jeon JH, Lee SJ, Yoon MY, et al. Intra-articular delivery of synovium-resident mesenchymal stem cells via BMP-7-loaded fibrous PLGA scaffolds for cartilage repair. *J Contr Release* 2019;302:169–80.
- Zhu S, Zhang B, Man C, Ma Y, Liu X, Hu J. Combined effects of connective tissue growth factor-modified bone marrow-derived mesenchymal stem cells and NaOH-treated PLGA scaffolds on the repair of articular cartilage defect in rabbits. *Cell Transplant* 2014;23(6):715–27.
- Sanjurjo-Rodríguez C, Castro-Viñuelas R, Hermida-Gómez T, Fuentes-Boquete IM, de Toro FJ, Blanco FJ, et al. Human cartilage engineering in an in vitro repair model using collagen scaffolds and mesenchymal stromal cells. *Int J Med Sci* 2017;14(12):1257–62.
- de Mulder ELW, Hannink G, van Kuppevelt TH, Daamen WF, Buma P. Similar hyaline-like cartilage repair of osteochondral defects in rabbits using isotropic and anisotropic collagen scaffolds. *J Tissue Eng Part A* 2014;20:3–4.
- Tamaddon M, Samizadeh S, Samizadeh S, Wang L, Blunn G, Liu C. Intrinsic osteoinductivity of porous titanium scaffold for bone tissue engineering. *Int J Biomater* 2017;10:1–11.
- Tilley JMR, Chaudhury S, Hakimi O, Carr AJ, Czernuszka JT. Tenocyte proliferation on collagen scaffolds protects against degradation and improves scaffold properties. *J Mater Sci Mater Med* 2012;23(3):823–33.
- Smith GD, Taylor J, Almqvist KF, Erggelet C, Knutsen G, Portabella MG, et al. Arthroscopic assessment of cartilage repair: a validation study of 2 scoring systems. *Arthroscopy* 2005;21(12):1462–7.
- Oliver WC, Pharr GM. An improved technique for determining hardness and elastic modulus using load and displacement sensing indentation experiments[J]. *J Mater Res* 1992;7(6):1564–83.
- Hu K, Radhakrishnan P, Patel RV, Mao JJ. Regional structural and viscoelastic properties of fibrocartilage upon dynamic nanoindentation of the articular condyle. *J Struct Biol* 2001;136(1):0–52.
- Yoshimura H, Muneta T, Nimura A, Yokoyama A, Koga H, Sekiya I. Comparison of rat mesenchymal stem cells derived from bone marrow, synovium, periosteum, adipose tissue, and muscle. *Cell Tissue Res* 2007;327(3):449–62.
- Li JJ, Kim K, Roohani-Esfahani S-I, Guo J, Kaplan DL, Zreiqat H. A biphasic scaffold based on silk and bioactive ceramic with stratified properties for osteochondral tissue regeneration. *J Mater Chem B* 2015;3(26):5361–76.
- Belu A, Mahoney C, Wormuth K. Chemical imaging of drug eluting coatings: combining surface analysis and confocal Raman microscopy. *J Contr Release* 2008;126:111–21.
- Liu C, Wang X, Zhang HJ, You X, Yue O. Self-healable, high-strength hydrogel electrode for flexible sensors and supercapacitors. *ACS Appl Mater Interfaces* 2021;13(30):36240–52.
- Zhang M, Lin R, Wang X, Xue J, Deng C, Feng C, et al. 3D printing of Haversian bone-mimicking scaffolds for multicellular delivery in bone regeneration. *Sci Adv* 2020;6(12):eaaz6725.
- Zhang B, Skelly JD, Maalouf JR, Ayers DC, Song J. Multifunctional scaffolds for facile implantation, spontaneous fixation, and accelerated long bone regeneration in rodents. *Sci Transl Med* 2019;11(502):eaau7411.
- Fujiwara N, Kobayashi K. Macrophages in inflammation. *Curr Drug Targets - Inflamm Allergy* 2005;4(3):281–6.
- Zhang F, Gao G, Wang P, Ye J, Huang Y, Wu H. The effect of PLGA-collagen I patch on inguinal hernia. *Farmacia* 2018;66(5):839–45.
- Zhang H, Huang H, Hao G, Zhang Y, Ding H, fan Z, et al. 3D printing hydrogel scaffolds with nanohydroxyapatite gradient to effectively repair osteochondral defects in rats. *Adv Funct Mater* 2020;2006697.
- Orth P, Cucchiariini M, Kohn D, Madry H. Alterations of the subchondral bone in osteochondral repair - translational data and clinical evidence. *Eur Cell Mater* 2013;25:299–316.
- Guo X, Park H, Young S, Kretlow JD, van den Beucken JJ, Baggett LS, et al. Repair of osteochondral defects with biodegradable hydrogel composites encapsulating marrow mesenchymal stem cells in a rabbit model. *Acta Biomater* 2010;6:39–47.
- Lin D, Cai B, Wang L, Cai L, Wang Z, Xie J, et al. A viscoelastic PEGylated poly(glycerol sebacate)-based bilayer scaffold for cartilage regeneration in full-thickness osteochondral defect. *Biomaterials* 2020;253:120095.
- Shieh AC, Athanasiou KA. Principles of cell mechanics for cartilage tissue engineering. *Ann Biomed Eng* 2003;31(1):1–11.